

Article

Improving the Protective Properties of Shellac-Based Varnishes by Functionalized Nanoparticles

Maduka L. Weththimuni ^{1,2}, Chiara Milanese ¹, Maurizio Licchelli ^{1,2,*} and Marco Malagodi ^{2,3}¹ Dipartimento di Chimica, Università di Pavia, 27100 Pavia, Italy;

madukalankani.weththimuni@unipv.it (M.L.W.); chiara.milanese@unipv.it (C.M.)

² Centro Interdipartimentale di Studi e Ricerche per la Conservazione del Patrimonio culturale, CISRiC, Università di Pavia, 27100 Pavia, Italy; marco.malagodi@unipv.it³ Dipartimento di Musicologia e Beni Culturali, Università di Pavia, 26100 Cremona, Italy

* Correspondence: maurizio.licchelli@unipv.it; Tel.: +39-0382-987-936

Abstract: Shellac is a natural varnish still known as one of the most elegant finishes for furniture and musical instruments, and currently used for restoration and refinishing of wooden antiques. However, it displays some limitations such as (i) sensitivity to alcoholic solvents (ii) softness of the coating, and (iii) considerable weathering due to photo- and bio-degradation. Hence, the main aim of this study was to improve the properties of shellac-based finish by introducing functionalized nanoparticles. Two inorganic nano-sized materials were considered: ZnO that was expected to reduce photo- and bio-degradation problems, and ZrO₂ that was expected to improve the hardness of the varnish. Nanoparticles were synthesized and treated with a bifunctional silane coupling agent. Both plain and functionalized nanoparticles were extensively characterized using different experimental techniques. Functionalized nanoparticles were grafted on shellac through a reaction involving the epoxy-rings introduced on their surface. The resulting modified varnishes were applied on maple wood specimens according to traditional procedures. Different instrumental techniques and testing methods were used to characterize both nano-sized materials and the corresponding nanocomposites, as well as to evaluate the performance of the new coatings. The investigated composite materials display the same aesthetic appearance as plain shellac, while some other properties were improved. In particular, both nanocomposites are distinctly less soluble in alcohols than plain shellac and display antifungal properties. Moreover, coating containing functionalized ZnO nanoparticles displays photo-protection behavior, while shellac modified with ZrO₂ nanoparticles exhibits a higher hardness when compared to the traditional varnish.

Keywords: shellac; wood protection; nanoparticles; GPTMS; zinc oxide; zirconium dioxide; SEM-EDS

Citation: Weththimuni, M.L.; Milanese, C.; Licchelli, M.; Malagodi, M. Improving the Protective Properties of Shellac-Based Varnishes by Functionalized Nanoparticles. *Coatings* **2021**, *11*, 419. <https://doi.org/10.3390/coatings11040419>

Academic Editor: Marko Petric

Received: 6 March 2021

Accepted: 1 April 2021

Published: 4 April 2021

Publisher's Note: MDPI stays neutral with regard to jurisdictional claims in published maps and institutional affiliations.



Copyright: © 2021 by the authors. Licensee MDPI, Basel, Switzerland. This article is an open access article distributed under the terms and conditions of the Creative Commons Attribution (CC BY) license (<https://creativecommons.org/licenses/by/4.0/>).

1. Introduction

Surface coating is the most common method used to protect wood against deterioration and improve and stabilize its distinctive appearance. Shellac (SH) is a natural polymer and one of the thermosetting resin of animal origin secreted by the lac insects (e.g., *Kerria lacca*, *Laccifer lacca*) [1–3]. Shellac has been widely used as a protective material for wooden furniture and musical instruments, due to its excellent properties such as ease of application, high adhesion to the wood surface, and protective properties along with its non-poisonous nature [3–5]. Moreover, it is still known as one of the most elegant finishes for furniture and currently used for restoration, conservation of wooden artifacts, and refinishing wooden antiques [3,6,7]. In particular, shellac is one of the most used varnishes for string musical instruments [3,8]. Despite these advantages, the uses of shellac have significantly declined, because of some limitations such as the softness of the coating, sensitivity to photodegradation and to alcoholic solvents [3,5,9]. In recent years, introduction of cross-linking agents [4,10] or of inorganic nanoparticles [3] have been reported as promising methods to improve the performances of shellac in different applications, including the

resistance of shellac-based varnishes when exposed to aggressive agents (light, solvents, scratches). Nano-sized materials, particularly nanoparticles (NPs), have been recently tested in the Cultural Heritage conservation field, for instance as photo-protective and anti-microbial agents [11,12]. Various nanomaterials such as metal NPs (gold, copper and silver) and different metal oxide NPs are currently used in the preservation and restoration treatments of different heritage objects [11].

Based on the above, and following our interest in the development of new materials for the preservation of cultural heritage items [3,5,13,14] we decided to further investigate the effect of nanoparticles in the shellac-based varnishes.

Although inorganic NPs simply dispersed in the resin can provide promising results [3], it should be considered that they may progressively migrate through the coating matrix after application, inducing aggregation phenomena and performance loss over time. This possible drawback can be faced by using nano-sized materials that have been appropriately modified in order to avoid or reduce possible migration and/or aggregation phenomena. In fact, as reported in literature, surface grafting/functionalization of nanoparticles with organic compounds can improve the dispersion of the NPs as well as prevent their aggregation and migration in polymer matrixes [15,16].

The present investigation aimed to improve the properties of the traditional shellac varnish by incorporating properly functionalized inorganic NPs into the resin. Two different types of nanoparticle, namely ZnO and ZrO₂, were chosen considering their excellent properties. In particular, ZnO was expected to reduce photo- as well as bio-deterioration problems of the shellac matrix, while ZrO₂ was added with the aim of improving the film hardness.

Zinc oxide, ZnO, is a semiconductive material that has attracted great interest in different research fields due to its excellent properties together with its non-toxic and environmentally friendly behavior. Hence, ZnO NPs have been widely applied, e.g., in the preparation of photo-catalysts, solar cells, chemical sensors, piezoelectric transducers, transparent electrodes, electroluminescent devices and gas sensors, electrostatic dissipative coating, ultraviolet laser diodes [15,17–19]. Among oxide nanoparticles, nano-sized ZrO₂ is an attractive material too, due to some interesting properties, such as chemical inertness, excellent thermal stability, high refractive index and high hardness [16]. Therefore, ZrO₂ has been used in a variety of industrial and engineering applications that include high durability coating, catalytic agents, cutting tools, seals, valves and tiles for space shuttles and missiles, turbines, and the most demanding aviation engines [20–23].

Surface functionalization of inorganic fillers by an organic agent, beside reducing re-aggregation phenomena, is usually an effective way to enhance the compatibility between organic and inorganic phases. Furthermore, the functionalization of nanoparticles with organic compounds represents a method for properly activating the NPs surface in order to fit the target applications [15–17,24,25]. Silane coupling agents are commonly used for the functionalization of different oxide NPs [16,26–29]. The bifunctional silane 3-glycidoxypropyltrimethoxysilane (GPTMS) containing a reactive organic epoxide in addition to the hydrolyzable methoxysilane group, has been extensively applied to functionalize inorganic NPs. In fact, owing to its features, GPTMS may react with both inorganic and organic compounds, behaving as an efficient surface modifier [16,26,30]. In this research work, this coupling agent was indeed chosen for its dual reactivity: methoxysilane groups of GPTMS can be exploited to functionalize the surface of the envisaged inorganic NPs through the condensation involving –OH functions on the oxide surface, while epoxy functionality is suitable to link NPs to the organic varnish matrix. In fact, carboxylic groups present in shellac structure are expected to react with GPTMS by the opening of the epoxide ring. As a result, nanoparticles can be covalently linked to shellac backbone, and, at the same time, a partial cross-linking of the varnish can take place. The peculiar properties of inorganic NPs (i.e., ZnO and ZrO₂) combined with the possible cross-linking are expected to positively affect the properties of native shellac.

Therefore, the main aim of this work was to prepare new shellac-based varnishes containing functionalized inorganic nanoparticles, which display improved performances compared to plain shellac (e.g., resistance to alcohol, hardness, photostability, resistance to fungal attack). To achieve this purpose we planned the following steps: (i) preparation of ZnO and ZrO₂ nanoparticles functionalized with 3-glycidoxypropyltrimethoxysilane, (GPTMS); (ii) preparation of nanocomposites by reacting dewaxed shellac with functionalized inorganic NPs; (iii) evaluation of modified shellac properties in comparison with the plain varnish. Different instrumental techniques were used to characterize both nano-sized materials and the corresponding shellac derivatives, such as dynamic light scattering (DLS), X-ray powder diffractometry (XRPD), optical microscopy (OM), scanning electron microscopy (SEM), energy-dispersive X-ray spectroscopy (EDS), Fourier transform infrared spectroscopy (FTIR), thermogravimetric analysis (TGA) and differential scanning calorimetry (DSC). A variety of measurements and tests were also performed in order to assess the performances of the investigated varnishes, such as contact angle and chromatic variation measurements, hardness and solubility tests, as well as specific tests to evaluate the effects of ultraviolet (UV) induced ageing and fungi-induced biodeterioration.

2. Materials and Methods

2.1. Materials

Zinc acetate di-hydrate, Zn(CH₃COO)₂·2H₂O, and sodium hydroxide, NaOH, were purchased from Carlo Erba reagents. Zirconyl chloride octa-hydrate, ZrOCl₂·8H₂O, 3-glycidoxypropyltrimethoxysilane (C₉H₂₀O₅Si, GPTMS, ≥98%), Tetrahydrofuran (C₄H₈O, anhydrous THF, ≥99.9%) and ethanol (absolute EtOH, ≥99.8%) were supplied by Sigma-Aldrich. Deionized water was used during the synthesis of NPs. Moreover, dibutyltin dilaurate (C₃₂H₆₄O₄Sn, DBTL, 95%) were supplied by Fluka (Munich, Germany) and used as a catalyst. Dewaxed natural shellac (food quality) was purchased from Kremer Pigmente (Aichstetten, Germany) and used without any further purification. The wood specimens (provided by Rivolta srl company, Desio, Italy) were obtained by a single Maple tree (wood species: *Acer pseudoplatanus* L.) grown in Slovenia. The density of the wood (heartwood) was 0.58 ± 0.05 g/cm³. The specimens were conditioned for 21 days at 22 ± 2 °C and 54 ± 5% RH. The final moisture content was about 7%. Specimens used in the present work were 45, in total, and their dimensions were 5 × 5 × 0.5 cm³ (tangential/longitudinal/radial, respectively).

2.2. Synthesis and Characterization of Functionalized Nanoparticles

Plain ZnO and ZrO₂ NPs were synthesized according to the literature methods, with slight modifications [20,31].

For ZnO NPs: NaOH dissolved in EtOH (50 mL, 0.3 M) was added dropwise into a round bottom flask containing a solution of Zn(CH₃COO)₂ in EtOH (50 mL, 0.2 M) with continuous magnetic stirring. The resulting mixture was heated and a white precipitate formed when the temperature reached 78.4 °C (boiling point of EtOH). After that, the solid product was washed several times with water (until the pH was 7) to remove residual sodium salt (CH₃COONa) and then with absolute EtOH. Finally, the product obtained was dried in an oven at 150 °C for several hours in order to obtain ZnO nanopowder.

For ZrO₂ NPs: NaOH aqueous solution (15 mL, 1 M) was added dropwise into a round bottom flask containing an aqueous solution of ZrOCl₂·8H₂O (50 mL, 0.1 M) with continuous magnetic stirring. The temperature of the resulting mixture was set at 80 °C. After obtaining a white precipitate, it was centrifuged and washed with deionized water and then dried in an oven at 150 °C for several hours.

Synthesized NPs were functionalized with GPTMS by adapting a method from the literature [32]. For this purpose, NPs (1.0 g, either ZnO or ZrO₂) were suspended in anhydrous THF (20.0 mL) by using an ultrasonic bath. The suspension was transferred into a 100 mL round bottom flask containing GPTMS (2.0 mL) and anhydrous THF (5.0 mL). The reaction was carried out at 40 °C for 24 hours under dinitrogen atmosphere. At the

end of the reaction, the solution was centrifuged and resuspended in THF for several times in order to remove unreacted silane. Finally, the isolated product (either ZnO or ZrO₂ NPs) was dried in an oven at 90 °C. The functionalized nano-sized materials were labeled as ZnO-ES and ZrO₂-ES.

2.3. Synthesis of Varnishes

In order to obtain the nanocomposite materials (NPs-GPTMS grafted shellac varnish), the functionalized NPs (either ZnO-ES or ZrO₂-ES, 2%, *w/w* with respect to shellac: were mixed with the ethanolic solution of shellac (30 mL, 200 g/L) in the presence of dibutyltin dilaurate (DBTL, 0.5% *w/w* with respect to shellac) as a catalyst for the reaction involving carboxyl groups of the shellac and epoxide groups on the NPs surface. NPs percentage value (2%) was chosen on the basis of previous experiments [3]. In fact, larger amounts of both ZnO and ZrO₂ nanoparticles, when dispersed into shellac, induced perceptible color changes and turbidity problems. The resulting mixture was continuously stirred for 24 h, then it was treated by Ultrasonic Homogenizer (Badeline Sonoplus HD 2070, BANDELIN, Berlin, Germany; dispersion time: 5 min; power set at 50%). The resulting nanocomposites (shellac combined with functionalized NPs) were labelled as ZnO-ES-SH and ZrO₂-ES-SH, respectively, and readily used for the application on wood specimens and for the preparation of coating films.

2.4. Preparation of Coated Wood Samples and Coating Films

Both nanocomposites (ZnO-ES-SH and ZrO₂-ES-SH) and native shellac (SH) were applied to maple wood specimens as mentioned in our previous papers and in accordance with the method used by string instrument makers, particularly concerning the procedure of coating application by brushing [3,33,34]. In particular, wood specimens were smoothed by abrasive paper sheets (progressively from 400 to 1000 mesh, similarly to the procedure used by string instrument makers) and cleaned to remove dust [3,33]. The treatment was performed by consecutively applying the varnishes for 20 times with a special brush (Martora Kolinsky, Tintoretto, Arezzo, Italy) and the direction of brush in each application was perpendicular to the previous one in order to obtain, as much as possible, a regular coating surface. Most of the wood specimens were treated only on one square surface. Specimens intended to be used to test the antifungal activity of varnishes were completely coated. Moreover, films of the different varnishes were also prepared by casting, using polyvinyl chloride (PVC) sheets as well as glass slides (microscope slides) as supports. Finally, the wood specimens and the films were kept in the laboratory condition (T = 20 °C) for 3 weeks in order to fully dry the coatings before performing further analyses.

2.5. Instrumental Techniques and Testing Methods

Dynamic light scattering (DLS) measurements were performed by a MALVERN ZS90 apparatus (Malvern Panalytical Private Limited, Malvern, UK). Both NPs and doped NPs were well mixed in EtOH using an ultrasonic bath and then, 1 mL of each solution was put into the plastic stub. The measurements (time = 60 s) were performed at 25 °C. Moreover, the each analysis was repeated three times in order to get the accurate measurement.

X-ray powder diffraction (XRPD) measurements were taken using a Bruker D5005 diffractometer (Bruker Corporation, Billerica, MA, USA) with the CuK α radiation, graphite monochromator, and scintillation detector. The measurements were performed from 5° to 80° with step scan mode: scan step 0.02°, counting time 10 s per step; X-ray tube working conditions: 40 kV and 40 mA.

Infrared spectra were collected by a PerkinElmer Spectrum 100 Fourier transform infrared (FT-IR) spectrometer in the attenuated total reflectance (ATR) mode (PerkinElmer, Waltham, MA, USA). Well ground powder samples were used and spectra were obtained after pressing the sample towards the ATR diamond crystal at room temperature (20 °C). Moreover, three spectra for each sample were collected to obtain an average spectrum.

Optical microscope observations of wood specimens were performed by a light-polarized microscope Olympus BX51TF (Olympus Corporation, Tokyo, Japan), equipped with visible lamp (Olympus TH4-200).

Scanning electron microscopy (SEM) images (backscattered electron, BSE) and energy-dispersive X-ray spectra (EDS) were collected by using a Tescan FE-SEM Mira 3XMU-series (TESCAN, Brno, Czech Republic), equipped with a Schottky field emission source and with a Bruker Quantax 200 energy-dispersive X-ray spectrometer (EDX) (Bruker, Billerica, MA, USA), operating in both low and high vacuum and located at the Arvedi Laboratory, CISRIC, Università di Pavia. Before SEM-EDS analysis, samples were gold-sputtered using a Cressington sputter coater 208HR (Ted Pella, Inc., Redding, CA, USA).

Thermogravimetric (TGA) measurements were performed by a Q5000 apparatus (TA Instruments, New Castle, DE, USA) under nitrogen flux (10 ml/min) in a platinum pan by heating about 10 mg of sample from room temperature up to 700 °C (heating rate 5 K/min).

Differential scanning calorimetry (DSC) was performed by a Q2000 apparatus (TA Instruments, New Castle, DE, USA) by heating about 10 mg of powder in an open aluminium crucible from −50 °C to 250 °C (heating rate 5 K/min) under nitrogen flux (50 mL/min). Three independent measurements were taken on each sample. The temperature accuracy of the instrument is ± 0.1 °C, the precision is ± 0.01 °C, and the calorimetric reproducibility is $\pm 0.05\%$.

Solubility tests were performed according to a previously reported method [5]. Fully dry films (3 weeks after the preparation) were used. In particular, ethanol (16 mL) was added to glass vials containing small strips of each film (0.5 g) and then, the vials were shaken for 1 h by a linear shaker. After that, insoluble fractions were isolated, dried and weighed.

Colour measurements were taken by using a Konica Minolta CM-2600d spectrophotometer (Konica Minolta, Inc., Tokyo, Japan), determining the L^* , a^* , and b^* coordinates of the CIELAB space, and the global chromatic variations expressed as ΔE^* values, according to the UNI EN 15886 protocol [35].

Static contact angle measurements were performed by a Lorentzen and Wettre instrument (Zurich, Sweden) according to the UNI EN 15802 Protocol [36].

Concerning color and contact angle measurements, three different wood specimens were used for each kind of treatments (SH, ZnO-ES-SH, and ZrO₂-ES-SH) and five measurements were taken on each specimen area, therefore, all the given results are average values from 15 measurements.

UV ageing tests were performed by using an irradiation system (Helios Italquartz, Milan, Italy) equipped with a couple of mercury lamps (15 W) for 500 h, as previously reported [34,37,38]. During the irradiation, temperature and relative humidity in the chamber were controlled at 25 °C and 30%, respectively. At the end of the experiment, the specimens were analyzed by measuring chromatic variations.

Antifungal performance was evaluated on wood specimens treated with the examined varnish (ZnO-ES-SH, ZrO₂-ES-SH, and SH, taken as a reference) according to a procedure from the literature [37,39]. Three different wood specimens were used to test each kind of coating. Maple specimens were water saturated (by immersion), and then they were placed in desiccators with controlled conditions (relative humidity and temperature set at $95 \pm 2\%$ and 24 ± 1 °C, respectively). The desiccators were kept in the laboratory with natural illumination in the day time and a dark break at night for 40 days. The presence of molds on each wood specimen was investigated every day and ultimately, they were examined by OM and SEM.

The pencil hardness test was performed both on wood specimens treated with ZrO₂-ES-SH and with plain SH as well as on the corresponding coating films, according to ISO15184:1998 standard [40].

3. Results and Discussion

3.1. Characterization of Nanoparticles (NPs) and Functionalized NPs

Plain and GPTMS-functionalized NPs were characterized by different techniques in order to gain information about their chemical compositions, sizes, and shapes.

DLS analyses (Figure S1) suggested that most of ZnO and ZrO₂ NPs (99%) were in the range size 30–110 nm and 90–230 nm, respectively. After functionalization, a slight increase of particle sizes was observed. In particular a size ranging between 70 and 160 nm was detected for ZnO-ES, while the diameter of ZrO₂-ES ranged between 100 and 320 nm.

The XRPD patterns (see Figure 1) showed the presence of zinc oxide and zirconium dioxide as the main components of the analyzed powders (ZnO and Zr₂O NPs, respectively). ZnO is in the form of hexagonal wurtzite (space group P 63 m c, JCPDS No. 96-230-0114) [15,41–43] and ZrO₂ is in the tetragonal polymorph (JCPDS No. 70-1769) [44,45]. The tetragonal (t) phase could be stabilized due to its lower surface energy if compared to the monoclinic (m) phase, which is generally the stable one at room temperature [20]. Similar diffraction patterns were observed even in the corresponding GPTMS-capped NPs, meaning that the functionalization with silane does not interfere on the crystal structure of the NPs [15,41].

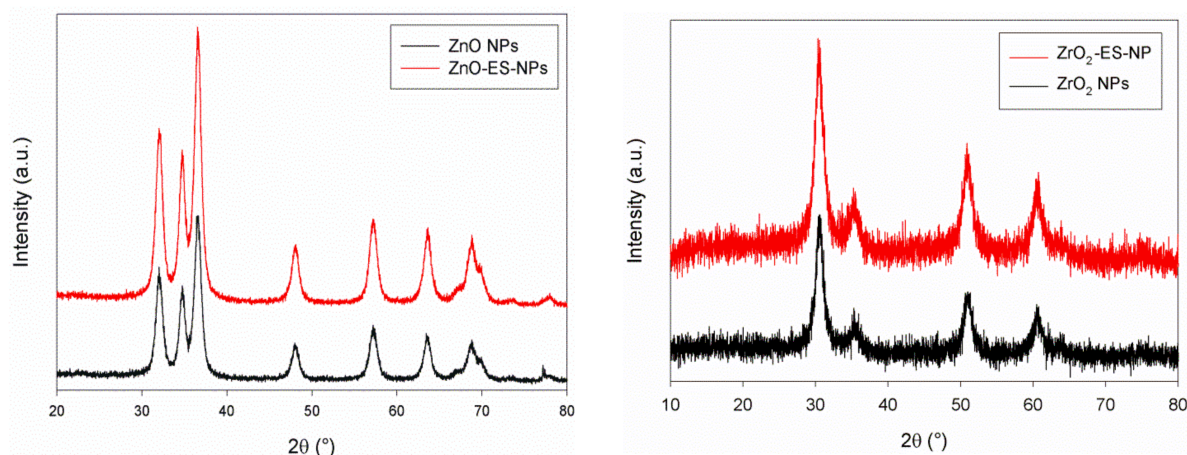


Figure 1. X-ray powder diffraction (XRPD) patterns of nanoparticles (NPs) and 3-glycidoxypropyltrimethoxysilane (GPTMS)-capped NPs: ZnO and ZnO-ES (left); ZrO₂ and ZrO₂-ES (right).

XRPD measurements also provided information about the size of both plain and functionalized NPs. According to the Scherrer equation, the size of ZnO particles ranges between 63 and 71 nm, while the size of ZnO-ES NPs is in the 26–56 nm range. Size values calculated for ZrO₂ NPs are in the 51–93 nm range, and they drop down to 43–60 nm after silane grafting (Zr + ES). According to the XRPD data, the sizes of plain NPs are larger than the functionalized NPs both for ZnO and Zr₂O. This behaviour may be ascribed to the prevention of agglomerations due to the surface functionalization of NPs.

SEM observations showed that the particles contained in ZnO powder have a roundish shape with a size mostly ranging between 40 and 80 nm (Figure 2a) [17,31]. A similar shape and an about 20–60 nm size range was observed in the case of ZnO-ES (Figure 2b). Some larger particles formed by aggregates of quite spherical smaller subunits were also observed both for plain and functionalized ZnO NPs (Figure 2a,b). Microanalyses performed by EDS confirmed the expected elemental composition of the nano-sized materials. In particular, EDS spectrum of plain zinc oxide NPs showed only the peaks corresponding to Zn and O while the presence of C and Si due to the surface functionalization by GPTMS is clearly observed in ZnO-ES, in addition to the main components (Figure 2a,b, insets).

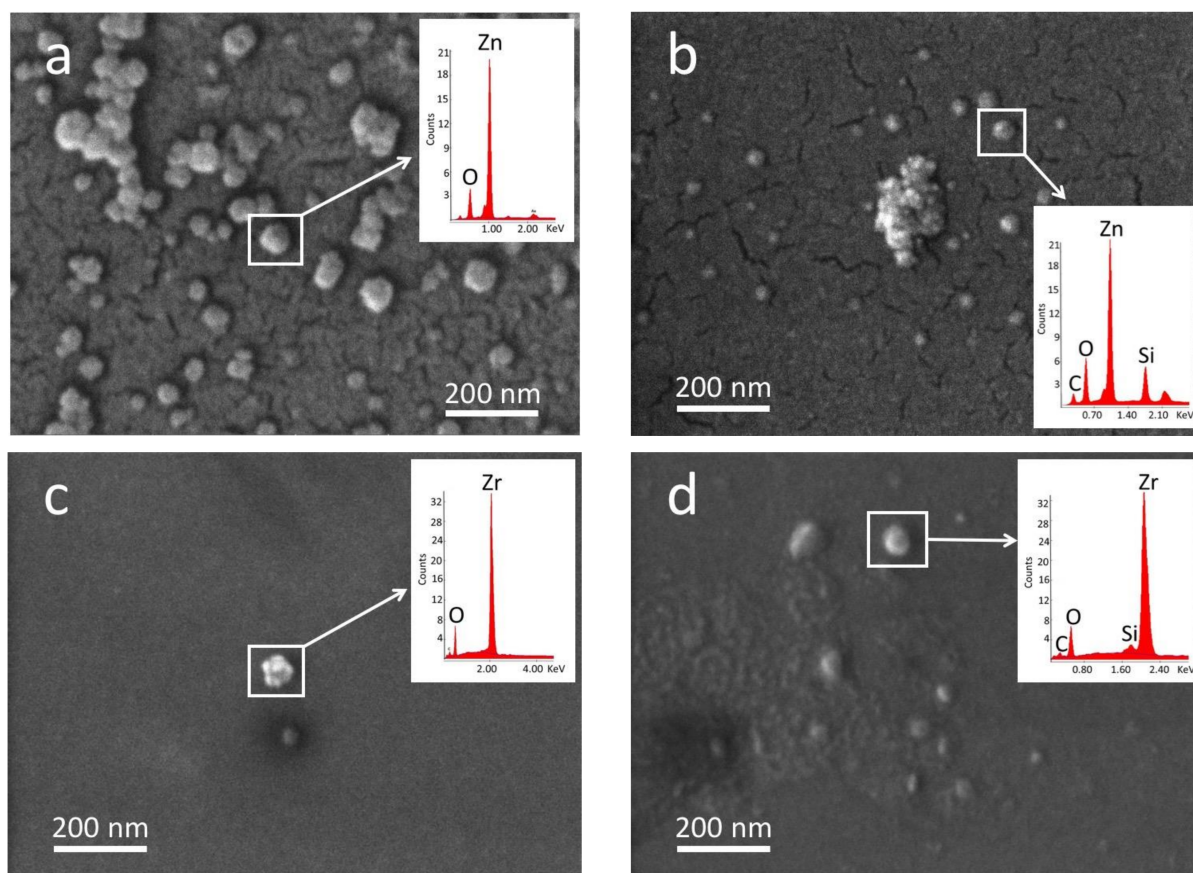


Figure 2. Scanning electron microscopy (SEM) micrographs of investigated NPs and GPTMS-capped NPs: (a) ZnO; (b) ZnO-ES; (c) ZrO₂; (d) ZrO₂-ES. Corresponding EDS spectra are in the insets; Au peaks (2.1–2.2 KeV) in the spectra are due to gold sputtering of the samples.

According to SEM images, ZrO₂ NPs mainly have a rounded appearance [20,46] with their sizes roughly ranging between 40 and 140 nm, although several particles are actually made by aggregates of smaller entities (Figure 2c). Moreover, some larger particles display also hexagonal shape (see Figure S2) similar to what has been already observed for other nano-sized zirconia-based materials [47]. ZrO₂-ES NPs also display almost spherical shapes whose dimensions approximately range between 30 and 100 nm. EDS spectra confirmed the composition of zirconia NPs (Zr and O peaks only) and demonstrated the presence of the grafted silane moieties on the surface of ZrO₂-ES NPs, since the peaks of C and Si were observed in addition to the main elemental components (Figure 2c,d, insets).

Taking into account the results of the XRPD and SEM experiments, it is worth noting that the functionalization of inorganic NPs with epoxysilane does not affect to a great extent their size and shape. In particular XRPD data indicate that GPTMS grafting on the surface of NPs induce a small reduction of their average size, which could be explained in terms of inhibition of the aggregation process. Anyway, agglomeration of plain as well as functionalized NPs cannot be ruled out at all, as demonstrated by SEM observations, which clearly show some large particles composed of several spherical aggregated subunits. Moreover, size ranges determined by DLS experiments for all investigated NPs are wider than the corresponding ranges obtained by the other techniques, suggesting that some aggregation processes can take place in the investigated EtOH suspensions.

In order to investigate the chemical composition of NPs before and after grafting and particularly to point out the presence of organic moieties on their surface, FTIR analyses (ATR mode) were also undertaken on powder samples and on GPTMS, taken as a reference. The spectra collected for all the examined materials are reported in Figure 3.

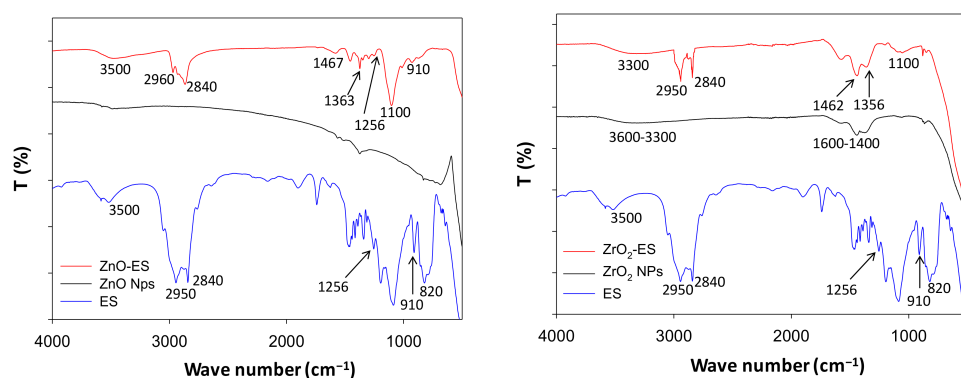


Figure 3. Fourier transform infrared (FTIR) spectra (attenuated total reflectance (ATR) mode) of NPs and GPTMS-capped NPs: ZnO (left) and ZrO₂ (right); spectrum of 3-glycidoxypropyltrimethoxysilane (ES) is also reported for comparison.

The spectrum of plain ZnO NPs does not display significant bands in the 4000–800 cm^{−1} range [48]. The expected broadband at 472 cm^{−1} due to Zn–O stretching [15,49] is out of the usable wavenumber range and cannot be detected. The spectrum of ZnO-ES powder exhibits several signals, the most intense being at 3000–2800 cm^{−1} and at about 1100 cm^{−1}, which can be ascribed to the stretching of C–H bonds in the side chain of the grafted silane and to Si–O bond, respectively. Other, less intense peaks observed in the 1500–1200 cm^{−1} region can be ascribed to C–H (bending modes) and to C–O bond of the grafted organic chains. Comparison with the spectrum of unreacted GPTMS also indicates that the distinctive peaks of the epoxide group at 1256 and 910 cm^{−1} (due to symmetric and asymmetric deformation of the oxirane ring [16]) are still present in the spectrum of ZnO-ES.

ZrO₂ powder displays a very broad band in the 3600–3300 cm^{−1} range and other broad bands between 1600 and 1400 cm^{−1}, which can be ascribed to the surface O–H groups (stretching and bending, respectively) and to the presence of adsorbed moisture. The spectrum of functionalized ZrO₂ nanoparticles displays two peaks at 2950–2840 cm^{−1} (C–H stretching) and of a broad band around 1100 cm^{−1}, in the region where the signal of the Si–O bond is expected, suggesting that silane moiety is anchored on the NPs surface [16,50]. Differently from ZnO case, the two peaks typical of oxirane derivatives (expected at about 1260 and 910 cm^{−1}) cannot be clearly detected in the ZrO₂ spectrum, probably because they are obscured by the other broader bands in the same wavenumber range. The peak at about 820 cm^{−1} that has been ascribed to Si–O–CH₃ in the spectrum of GPTMS [48,51] almost completely disappears in the spectra of ZnO-ES and ZrO₂-ES, suggesting that the reaction of methoxysilane groups with –OH functions of NPs has taken place.

Results of FTIR investigations are substantially in agreement with data obtained by SEM-EDS and confirm the functionalization of the inorganic NPs with the organic moiety deriving from GPTMS.

Thermogravimetric analyses showed that plain NPs and their GPTMS-capped derivatives are stable up to 150 °C subsequently showing a mass loss, that correctly increases by heating up to 1000 °C from about 5 wt% for the pure NPs to 10 wt% of the treated ones due to the presence of the organic fraction. In the calorimetric profiles, no evident signals are evident up to 350 °C, confirming the stability of all the examined materials.

3.2. Characterization of Coatings

In order to understand the properties of modified varnishes (ZnO-ES-SH and ZrO₂-ES-SH) with respect to the natural shellac (SH), experimental analyses were done on both coating films and coated wood specimens.

3.2.1. Coating Films

Solubility tests on varnish films were performed to evaluate the resistance of modified shellac towards ethanol with respect to the native shellac. Plain varnish displays an almost

complete solubility in EtOH in the experimental condition of the test, as indicated by the low amount (about 17%) of insoluble residue. Owing to its organic nature, shellac is indeed expected to exhibit considerable solubility in organic solvents, particularly in alcoholic media [5,10]. By contrast, both varnishes obtained by modified shellac (ZnO-ES-SH, and ZrO₂-ES-SH) show improved resistance to ethanol after 3 weeks from the film preparation, as indicated by the larger amount of insoluble fraction (more than 60%, Figure S3, Table 1) detected at the end of the tests. This observation suggests that an irreversible modification takes place as a result of functionalization of native shellac with GPTMS-grafted NPs. In fact, the epoxide ring of the GPTMS moieties on the NPs surface may react with carboxylate groups of different shellac chains, providing a partial cross-linking that induces a solubility decrease of coating films in EtOH. The reaction involving carboxylate and epoxide groups is well-known [52–54] and in a few cases it has been exploited to cure or functionalize shellac [55,56]. Although the high solubility of shellac in alcohols can be considered as an advantage for users (e.g., easy application and/or removal of old coatings), the sensitivity to alcoholic solvents is a drawback for a shellac finish, because it can be damaged even by short contact with alcoholic compounds (for instance perfumes, alcoholic beverages). Therefore, increasing the resistance towards alcoholic solvents is an important property of shellac-based varnishes, because it gives long term protection to the finish.

Table 1. Glass transition temperatures determined for coating films and their insoluble fractions in alcohols (three independent measurements on each sample were done in order to obtain the average values).

Films	T _g /°C	Insoluble Fraction in EtOH (%)
SH	112 (±1)	17 (±6)
ZnO-ES-SH	108 (±1)	73 (±10)
ZrO ₂ -ES-SH	105 (±1)	72 (±6)

The thermal properties of plain shellac and of the modified varnishes were investigated by performing TGA and DSC analyses on films of SH, ZnO-ES-SH, and ZrO₂-ES-SH coatings.

Concerning the shellac-NPs composites, the comparison of their thermogravimetric profiles with the one recorded for pure shellac indicates that the NPs have a moderate stabilizing effect (Figure 4). In fact, the starting degradation temperatures of the two nano-composites is higher than the plain SH for each degradation recorded step. The effect is almost similar for the 2 metal oxides, although the curve of ZrO₂-ES-SH is shifted at a higher temperature than ZnO-ES-SH up to about 400 °C.

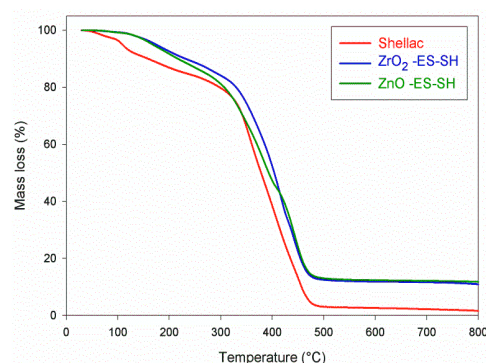


Figure 4. Thermogravimetric analysis profiles of plain shellac (SH) and of the nanocomposites ZnO-ES-SH and ZrO₂-ES-SH.

In the calorimetric profiles of the three samples, only the glass transition (T_g) can be observed up to 350 °C, whose temperature value decreases from pure shellac to the samples containing oxide NPs (Figures S4–S6). In particular, the lowest T_g value is observed for ZrO₂-ES-SH, suggesting again that zirconium oxide NPs provide the highest stability

among the tested materials. Decreasing T_g upon functionalization of shellac, although with different organic moieties, has been already reported [10,57].

3.2.2. Treated Wood Specimens

Shellac, as has already been mentioned, has been used for centuries to varnish wooden artifacts because of its excellent features, including the ability to enhance the aesthetic appearance of wood surface. NPs dispersed into the coatings could affect this peculiar property of SH. Therefore, treated wood specimens were at first examined to evaluate chromatic variations induced by ZnO-ES-SH, and ZrO₂-ES-SH coatings in comparison with plain shellac. Colour changes expressed as ΔE^* values, which were observed after wood surface treatments are reported in Table 2. Overall color changes experienced by wood surface were very similar for all the examined specimens ($16.7 < \Delta E^* < 22.1$) and, in any case, the different specimens cannot be distinguished from each other by the naked eye on the basis of their colour. The chromatic variations induced by all coatings on the maple surface were mainly due to the increased value of b^* coordinate (related to the blue-to-yellow change), as expected based on the yellow colour of natural shellac.

Table 2. The chromatic variations and the contact angle measurements of wood specimens after treatments and ultraviolet (UV) ageing. All data are average values from 15 measurements (three different wood specimens for each and every treatment and 5 measurements on each specimen).

Varnishes	After Treatments		After UV Ageing	
	$\Delta E^* (a)$	$\alpha (^\circ)$	$\Delta E^* (b)$	$\alpha (^\circ)$
SH	20.9 (± 1.2)	73 (± 4)	17.3 (± 0.3)	65 (± 2)
ZnO-ES-SH	16.7 (± 0.1)	91 (± 7)	8.6 (± 0.6)	87 (± 3)
ZrO ₂ -ES-SH	22.1 (± 0.3)	104 (± 5)	13.8 (± 0.3)	95 (± 2)

^(a) Overall chromatic variation referred to plain wood specimen. ^(b) Overall chromatic variation referred to unaged treated specimens.

Wood coatings are expected to provide protection also from environmental humidity. Therefore, the hydrophobic behaviour of the investigated shellac-based materials was evaluated by performing static contact angle measurements on the surface of treated maple specimens (Table 2). Plain shellac coatings usually display a weak-to-moderate hydrophobic character [3,58,59], which was confirmed by the α value (73°, this work) measured on the specimens coated with the native resin. A considerable increasing of α was observed in specimens coated with both ZnO-ES-SH, and ZrO₂-ES-SH (91° and 104°, respectively), suggesting that modification of the resin matrix due to functionalized NPs induced a significant improvement of the local water-repellence behaviour exhibited by shellac varnish.

These outcomes indicate that chromatic features of shellac varnish on wood are preserved despite the presence of functionalized NPs, while its hygroscopic behaviour is even improved.

In order to have a better insight on the microscopic properties of the coatings, wood specimens treated with SH, ZnO-ES-SH, and ZrO₂-ES-SH were investigated by electron microscopy. Selected SEM micrographs taken on the surface of the examined specimens are shown in Figure 5.

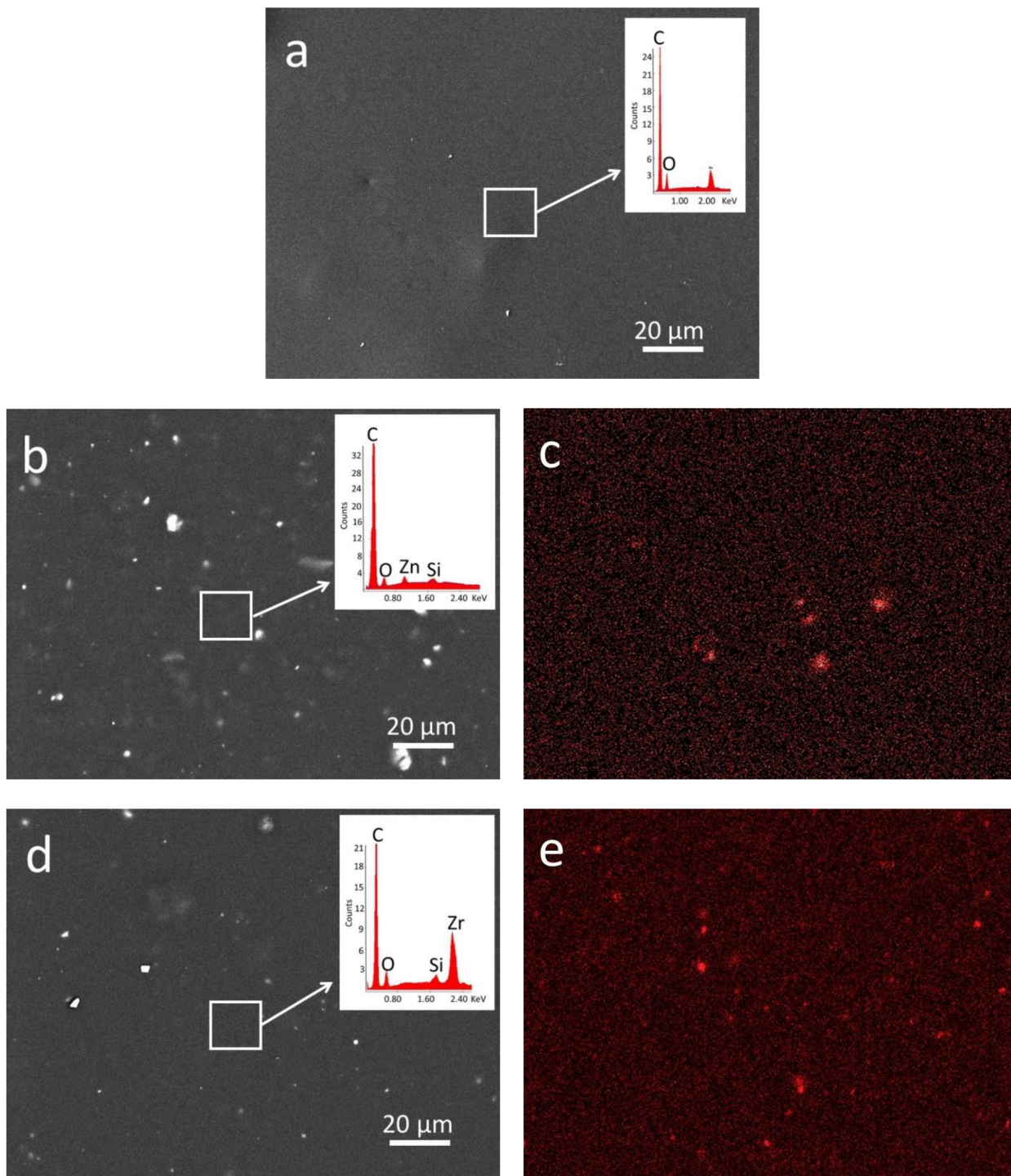


Figure 5. SEM micrographs of treated wood specimens: (a) SH; (b) ZnO-ES-SH and (c) the corresponding energy-dispersive X-ray spectroscopy (EDS) elemental mapping of zinc; (d) ZrO₂-ES-SH and (e) the corresponding EDS elemental mapping of zirconium. Selected EDS spectra are shown in the insets of SEM images. Au peaks (2.1–2.2 KeV) in the spectra are due to gold sputtering of the samples. High concentrations of Zn or Zr (and of the corresponding nanoparticles) are represented by red spots in the maps.

The surface of SH coating was very homogeneous: rare bright spots that were observed can be ascribed to occasional dust grains deposited as the varnish was drying. On the contrary, the examined areas of ZnO-ES-SH and ZrO₂-ES-SH coatings display the presence of widespread whitish spots which can be ascribed to the inorganic NPs, although the contribution of occasional dust grains cannot be ruled out, as suggested by some irregular very bright spots. The rather homogeneous distribution of NPs into the shellac matrix was

confirmed by EDS analyses carried out on the same areas observed by SEM (Figure 5b,d, insets). In particular, the EDS spectrum taken on ZnO-ES-SH coating displays not only the peaks due to C and O, main elemental components of shellac, but also peaks corresponding to Zn and Si that are the elements expected in the silane-functionalized ZnO NPs. Similarly, the peaks due to Zr and Si were observed in the EDS spectrum measured on the surface of the ZrO₂-ES-SH coating, in addition to the signals corresponding to C and O. It should be noted that the broad peak centered at about 2.1 keV ascribed to zirconium actually results from the overlapping of Zr-La and Au-M peaks (2.042 and 2.120 keV, respectively) [60]. In fact, all the examined samples were gold-sputtered prior to carrying out the SEM-EDS experiments and, as a consequence the Au-M peak can be observed in all EDS spectra. However, the correct identification of Zr can be performed by using a proper peak-fitting technique [61].

The distribution of GPTMS-grafted NPs in the organic matrix was also investigated by EDS elemental mapping experiments performed on treated specimens. Zinc and zirconium distribution maps obtained by analysing wood surfaces treated with ZnO-ES-SH and ZrO₂-ES-SH are reported in Figure 5c,e, respectively. Zn and Zr-containing nanoparticles (represented as red spots) are quite homogeneously dispersed into the organic resin, although some larger spots, possibly due to aggregated particles, can be also observed in the elemental maps.

3.3. Performances of Coatings

Shellac-based nanocomposites were examined by specific tests in order to evaluate the performances of the corresponding coatings applied on the wood surface, in comparison with the plain resin. In particular, surface hardness was evaluated for ZrO₂-ES-SH, while resistance to degradation induced by UV irradiation and antifungal features were investigated for the specimens coated with ZnO-ES-SH.

Hardness of wood coatings represents an important parameter when protective effectiveness from mechanical decay such as scratching is required. In order to evaluate the hardness properties due to the modification of native shellac by functionalized NPs, pencil tests on wood specimens treated with both ZnO-ES-SH and ZrO₂-ES-SH as well as on the corresponding coating films were performed. Reproducible results were obtained from the measurements that were repeated three times both on plain and modified shellac (three different wood specimens as well as films for each kind of treatments were used in order to provide average values). They are summarized in Table 3.

Table 3. The results of the pencil hardness test.

Varnishes	Films	Wood Specimens
SH	F	F
ZnO-ES-SH	H	H
ZrO ₂ -ES-SH	3H	3H

According to the pencil test, hardness of plain shellac coating corresponds to the intermediate level “F” in the scale ranging between 9B (softer) and 9H (harder) [62]. The same results were obtained for each examined coating when testing both treated wood specimens and the corresponding coating film samples. It is noteworthy that the coatings formed by modified shellac display an increased hardness compared to the plain varnish, particularly in the case of ZrO₂-ES-SH, which provided the hardest material (“3H”). In the case of Zn-ES-SH, the introduction of inorganic NPs induced only a moderate enhancement of shellac coating hardness (from “F” to “H” in the hardness scale).

Shellac usually undergoes alteration when exposed for a long time to sunlight, particularly due to its UV component [57]. Photo-oxidation and other light-induced chemical reactions, cause variations in the physico-chemical and mechanical properties of the biopolymer [63]. The alterations include chromatic changes whose intensity are commonly related to the photo-degradation extent.

Therefore, indirect evaluation of decay induced on shellac-based varnishes were evaluated by performing measurements of colour changes experienced by plain and modified shellac after light exposure. Maple specimens treated with shellac and modified shellac (6 specimens for each coating), were irradiated by UV lamp up to 500 h in order to simulate the naturally occurring photo-degradation processes. The variations of the chromatic coordinates detected after the irradiation cycle are graphically summarized in Figure 6.

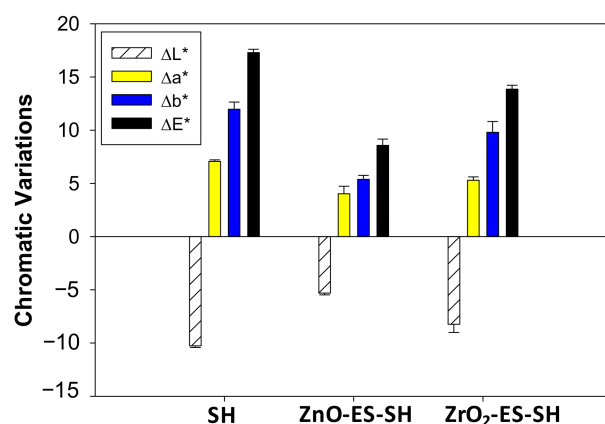


Figure 6. Chromatic variations experienced by wood specimens coated with SH, Zn-ES-SH, and ZrO₂-ES-SH after ultraviolet (UV) irradiation (500 h).

The UV irradiation of plain shellac coating mainly affects b^* and L^* parameters, related to the blue/yellow chromatic change and to the brightness, respectively. The value of a^* (the parameter related to chromatic changes towards the red) is affected to a lower extent. In particular, accelerated ageing induces a chromatic change towards the yellow, (positive Δb^* value) and a decrease of the surface brightness (negative ΔL^* value). As a consequence, a considerable chromatic variation ($\Delta E^* \sim 17$) was observed when comparing SH specimens after UV irradiation to the corresponding non-aged shellac coating (see Table 1). In the case of the nanocomposite containing ZnO nanoparticles, all chromatic coordinates undergo less intense variations due to UV-aging than the plain shellac, as graphically summarized in Figure 6. In particular, a distinctly lower value of ΔE^* (~ 8) was observed for ZnO-ES-SH (Table 2), suggesting that the modified shellac is more resistant toward the photo-degradation induced by UV light. This behavior can be ascribed to the well-known efficiency of ZnO as UV absorber, particularly when it is applied as nano-sized particles, as previously reported [37,62,64]. Coating containing ZrO₂ NPs undergoes less intense colour variation ($\Delta E^* \sim 13$) than shellac, but its performance is considerably worse than ZnO-ES-SH, in agreement with similar results reported in a previous paper [3].

In order to assess possible effects of photo-induced ageing on the hydrophobic properties of varnishes, contact angle measurements were also performed. A slight, albeit detectable, decrease of observed in the case of SH and ZrO₂-ES-SH indicated that the natural resin and its zirconia-containing derivative are less water-repellant after being exposed to UV light. This could be explained by taking into account that photo-oxidation processes occurring under irradiation usually provide oxygen-containing polar groups and that ZrO₂ NPs, as expected, do not display any protective effect. By contrast, the hydrophobic behaviour of ZnO-ES-SH was not affected by the prolonged irradiation, as the differences of values measured before and after artificial ageing are within the experimental error.

The anti-fungal behavior of modified shellac varnish was investigated by monitoring the growth of common fungal species, i.e. mold, on the surface of treated maple specimens according to a literature procedure [39].

Mold growth was monitored by exposing water-saturated specimens (ZnO-ES-SH, ZrO₂-ES-SH, and SH) to controlled ambient conditions (constant temperature and relative humidity, and natural daylight) Optical (OM) observations were performed after 3 weeks

and at the end of the test (40 days) in order to check for the presence of mold on the wood surface. Moreover, SEM experiments were carried out at the end of the experiment to better characterize the fungal microorganisms. After 3 weeks, the appearance of mold was clearly observed on SH (Figure S7), while the surface of ZnO-ES-SH, ZrO₂-ES-SH did not show evidence of mold growth. In particular, ZnO-containing varnish was still free from fungi, even at the end of the experiment, i.e., after 40 days.

SEM micrographs taken on the surface of SH and ZnO-ES-SH specimens before and after 40 days are reported in Figure 7. At the end of the test, mold colonies are diffusely present on the surface of plain shellac (Figure 7b,c), while the surface of wood specimens treated with ZnO-ES-SH has the same appearance as before treatment (Figure 7d,e) and no structure ascribable to mold can be observed even at high magnification (Figure 7f).

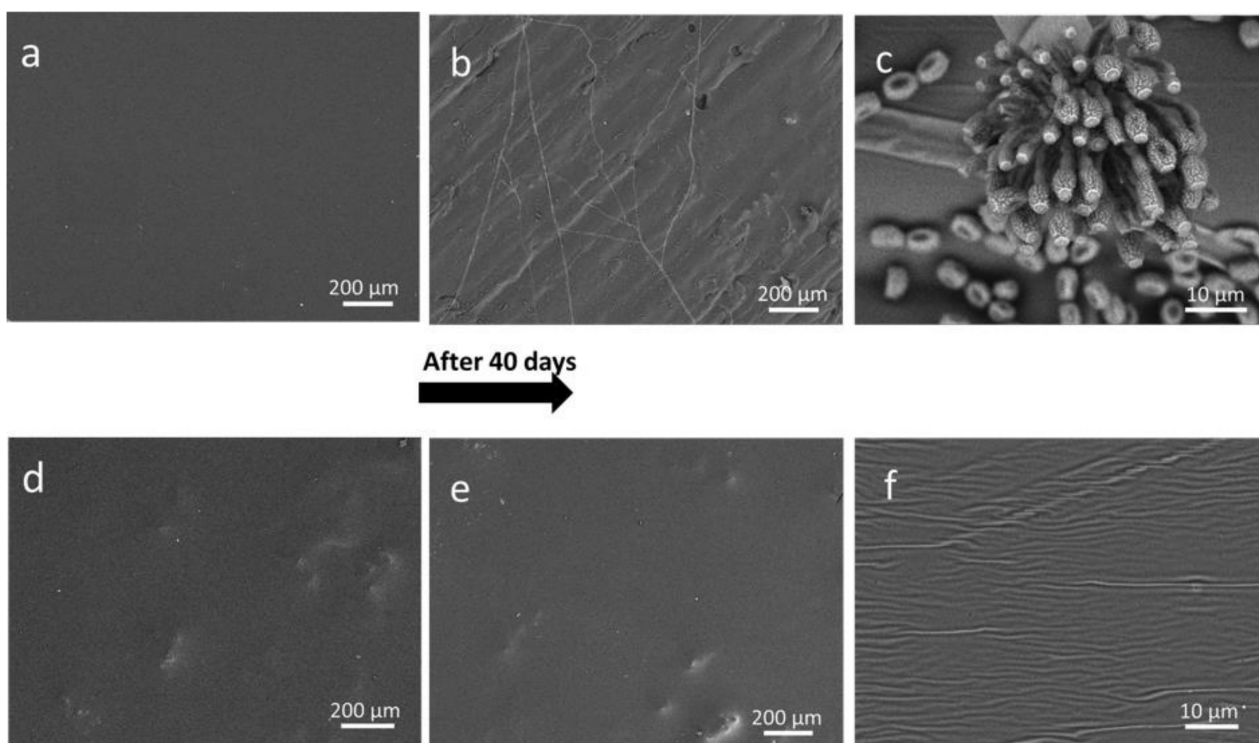


Figure 7. SEM micrographs taken on the surface of treated wood specimens during the fungi test: (a) SH before test; (b) SH after 40 days; (c) higher magnification of (b); (d) ZnO-ES-SH before test; (e) ZnO-ES-SH after 40 days; (f) higher magnification of (e).

These results confirm that the nano-sized ZnO behaves as anti-fungal agent in accordance with literature data [37,65–67] and that this feature is preserved even after functionalization. Although the antifungal effect of ZrO₂ has been investigated to a lower extent than ZnO [68,69], the results of the present study show that nano-sized zirconia, besides its numerous interesting properties, is also able to prevent the growth of mold on wood surface. As a consequence, shellac-based coatings containing ZnO-ES or ZrO₂-ES NPs display an increased resistance, when compared to plain shellac, toward biodeterioration induced by fungal agents and may improve the protection activity towards the wood substrate. Nevertheless, more research work is needed in order to assess the resistance of the modified coatings towards other biodeteriogens, e.g., some fungal species that specifically attack wood substrates.

4. Conclusions

In the present work inorganic nanoparticles (NPs) functionalized with 3-glycidoxypropyltrimethoxysilane (GPTMS) were prepared and used to provide chemically modified shellac varnishes. GPTMS-grafted ZnO and ZrO₂ NPs obtained after reaction of the inorganic nano-sized materials with the epoxysilane were characterized by SEM-EDS

and FTIR techniques, which confirmed the presence of organic functionalities on the NPs surface.

Varnishes prepared by dispersing GPTMS-grafted NPs (2%) into shellac (SH) provide coating films that display a good homogeneity and exhibit an improved resistance towards alcoholic media that usually damage shellac-based finish. The decreased solubility in ethanol can be ascribed to the partial cross-linking induced by reaction between oxyrane rings belonging to the organic moieties on the NPS surface and carboxylate groups of the natural resin.

The structural modification due to the partial curing process is also supported by thermal analyses, which show that the starting degradation temperatures of the two nanocomposites is higher than the plain SH. Interestingly, the modification of shellac with GPTMS-capped nanoparticles does not affect or affects to a poor extent the chromatic properties of the plain SH coating, while its water-repellence behaviour is even improved, as testified by contact angle measurements. Moreover, both the new coatings exhibit an enhanced resistance to alcoholic solvents. Varnish containing functionalized zirconia displays also a significantly increased resistance to scratches if compared to plain SH, as demonstrated by the surface hardness enhancement evaluated by the pencil test. On the other hand, modification of shellac induced by GPTMS-capped zinc oxide NPs provides a coating that displays an increased resistance towards ageing caused by UV irradiation and an enhanced resistance to common biodeteriogens (e.g., mold growth). Almost unexpectedly, a good antifungal behavior was observed also in the case of shellac modified with zirconia NPs.

In conclusion, this work has shown that the addition of the small amount (2%) of GPTMS-functionalized inorganic nanoparticles (ZnO and ZrO₂) to the traditional shellac varnish may induce relevant enhancement of its properties. Functionalization of NPs surface allows the inorganic particles to be fixed in the shellac matrix, preventing possible migration and/or aggregation processes that over time may cause loss of protecting effectiveness of the nanocomposite. In addition, the partial cross-linking of the natural resin can contribute to improving the varnish performance without negatively affecting the desirable features of native shellac (e.g., chromatic and water-repellence properties).

Supplementary Materials: The following are available online at <https://www.mdpi.com/2079-6412/11/4/419/s1>, Figure S1: Dynamic light scattering (DLS) analyses of synthesized nanoparticles (NPs) and 3-glycidoxypropyltrimethoxysilane (GPTMS)-capped NPs, respectively: (a) ZnO; (b) ZnO-ES; (c) ZrO₂; and (d) ZrO₂-ES; Figure S2: Scanning electron microscope (SEM) image of ZrO₂ NP displaying hexagonal shape; Figure S3: Insoluble fractions (%) of the varnish films in EtOH; Figure S4: Differential scanning calorimetry (DSC) profile obtained for plain shellac; Figure S5: DSC profile obtained for ZnO-ES-SH; Figure S6: DSC profile obtained for ZrO₂-ES-SH; Figure S7: Optical microscope images of treated wood specimens at the end of the fungi test: (a) shellac (SH); (b) ZnO-ES-SH; (c) ZrO₂-ES-SH.

Author Contributions: Conceptualization, M.L.; Data curation, M.L.W. and C.M.; Formal analysis, C.M. and M.M.; Investigation, M.L.W. and C.M.; Methodology, M.L.W. and C.M.; Resources, M.L.; Supervision, M.L.; Validation, M.L. and M.L.W.; Writing—original draft, M.L.W.; Writing—review & editing, M.L. All authors have read and agreed to the published version of the manuscript.

Funding: This research received no external funding.

Institutional Review Board Statement: Not applicable.

Informed Consent Statement: Not applicable.

Data Availability Statement: The data presented in this study are available in the present article and in the related Supplementary Information.

Acknowledgments: The authors would like to thank Claudio Carnevari for his kind guidance during the coating applications and Ilenia Tredici for assistance in SEM-EDS experiments.

Conflicts of Interest: The authors declare no conflict of interest.

References

1. Bose, P.K.; Sankaranarayanan, Y.; Sengupta, S.C. *Chemistry of Lac*; Indian Lac Research Institute: Ranchi, India, 1963.
2. Limmatvapirat, S.; Panchapornpon, D.; Limmatvapirat, C.; Nunthanid, J.; Luangtana-Anan, M.; Puttipipatkachorn, S. Formation of shellac succinate having improved enteric film properties through dry media reaction. *Eur. J. Pharm. Biopharm.* **2008**, *70*, 335–344. [[CrossRef](#)]
3. Weththimuni, M.L.; Capsoni, D.; Malagodi, M.; Milanese, C.; Licchelli, M. Shellac/nanoparticles dispersions as protective materials for wood. *Appl. Phys. A* **2016**, *122*, 1058–1069. [[CrossRef](#)]
4. Wang, J.; Chen, L.; He, Y. Preparation of environmental friendly coatings based on natural shellac modified by diamine and its applications for copper protection. *Prog. Org. Coat.* **2008**, *62*, 307–312. [[CrossRef](#)]
5. Licchelli, M.; Malagodi, M.; Somaini, M.; Weththimuni, M.; Zanchi, C. Surface treatments of wood by chemically modified shellac. *Surf. Eng.* **2013**, *29*, 121–127. [[CrossRef](#)]
6. Šimunková, K.; Pánek, M.; Zeidler, A. Comparison of selected properties of shellac varnish for restoration and polyurethane varnish for reconstruction of historical artefacts. *Coatings* **2018**, *8*, 119. [[CrossRef](#)]
7. Cook, W. *The Complete Guide to Repairing & Restoring Furniture*; Southwater: Leicester, UK, 2015; p. 256. ISBN1 10 1780191448. ISBN2 13 978-1780191447.
8. Nevin, A.; Echard, J.P.; Thoury, M.; Comelli, D.; Valentini, G.; Cubeddu, R. Excitation emission and time-resolved fluorescence spectroscopy of selected varnishes used in historical musical instruments. *Talanta* **2009**, *80*, 286–293. [[CrossRef](#)] [[PubMed](#)]
9. Limmatvapirat, S.; Nunthanid, J.; Luangtana-Anan, M.; Puttipipatkachorn, S. Effect of alkali treatment on properties of native shellac and stability of hydrolyzed shellac. *Pharm. Dev. Technol.* **2005**, *1*, 41–46. [[CrossRef](#)] [[PubMed](#)]
10. Otto, J.T.; Trumbo, D.L. A shellac derivative in thermoset coatings. *J. Coat. Technol. Res.* **2010**, *7*, 525–527. [[CrossRef](#)]
11. David, M.E.; Ion, R.M.; Grigorescu, R.M.; Iancu, L.; Andrei, E.R. Nanomaterials used in conservation and restoration of cultural heritage: An up-to-date overview. *Materials* **2020**, *13*, 2064. [[CrossRef](#)] [[PubMed](#)]
12. Fierascu, R.C.; Doni, M.; Fierascu, I. Selected aspects regarding the restoration/conservation of traditional wood and masonry building materials: A short overview of the last decade findings. *Appl. Sci.* **2020**, *10*, 1164. [[CrossRef](#)]
13. Licchelli, M.; Marzolla, S.J.; Poggi, A.; Zanchi, C. Crosslinked fluorinated polyurethanes for the protection of stone surfaces from graffiti. *J. Cult. Herit.* **2011**, *12*, 34–43. [[CrossRef](#)]
14. Licchelli, M.; Malagodi, M.; Weththimuni, M.; Zanchi, C. Nanoparticles for conservation of bio-calcareous stone. *Appl. Phys. A* **2014**, *114*, 673–683. [[CrossRef](#)]
15. Hong, R.Y.; Li, J.H.; Chen, L.L.; Liu, D.Q.; Li, H.Z.; Zheng, Y.; Ding, J. Synthesis, surface modification and photocatalytic property of ZnO nanoparticles. *Powder Technol.* **2009**, *189*, 426–432. [[CrossRef](#)]
16. Luo, K.; Zhou, S.; Wu, L.; Gu, G. Dispersion and functionalization of nonaqueous synthesized zirconia nanocrystals via attachment of silane coupling agents. *Langmuir* **2008**, *24*, 11497–11505. [[CrossRef](#)] [[PubMed](#)]
17. Hong, R.; Pan, T.; Qian, J.; Li, H. Synthesis and surface modification of ZnO nanoparticles. *Chem. Eng. J.* **2006**, *119*, 71–81. [[CrossRef](#)]
18. Wu, Y.L.; Tok, A.I.Y.; Boey, F.Y.C.; Zeng, X.T.; Zhang, X.H. Surface modification of ZnO nanocrystals. *App. Surf. Sci.* **2007**, *253*, 5473–5479. [[CrossRef](#)]
19. Faure, B.; Salazar-Alvarez, G.; Ahniyaz, A.; Villaluenga, I.; Berriozabal, G.; De Miguel, Y.R.; Bergström, L. Dispersion and surface functionalization of oxide nanoparticles for transparent photocatalytic and UV-protecting coatings and sunscreens. *Sci. Technol. Adv. Mater.* **2013**, *14*, 23001. [[CrossRef](#)] [[PubMed](#)]
20. Singh, A.K.; Nakate, U.T. Microwave Synthesis, Characterization, and Photoluminescence Properties of Nanocrystalline Zirconia. *Sci. World J.* **2014**, *2014*, 349457. [[CrossRef](#)]
21. Zhang, Q.; Shen, J.; Wang, J.; Wu, G.; Chen, L. Sol-gel derived ZrO₂-SiO₂ highly reflective coatings. *Int. J. Inorg. Mater.* **2000**, *2*, 319–323. [[CrossRef](#)]
22. Wright, P.K.; Evans, A.G. Mechanisms governing the performance of thermal barrier coating. *Curr. Opin. Solid. State. Mater. Sci.* **1999**, *4*, 25–30. [[CrossRef](#)]
23. Piconi, C.; Maccaro, G. Zirconia as a ceramic biomaterial. *Biomaterials* **1999**, *20*, 1–25. [[CrossRef](#)]
24. Sajjad, M.; Feichtenschlager, B.; Pabisch, S.; Svehla, J.; Koch, T.; Seidler, S.; Peterlik, H.; Kickelbick, G. Study of the effect of the concentration, size and surface chemistry of zirconia and silica nanoparticle fillers within an epoxy resin on the bulk properties of the resulting nanocomposites. *Polym. Int.* **2012**, *61*, 274–285. [[CrossRef](#)]
25. Hong, R.Y.; Qian, J.Z.; Cao, J.X. Synthesis and characterization of PMMA grafted ZnO nanoparticles. *Powder Technol.* **2006**, *163*, 160–168. [[CrossRef](#)]
26. Zhang, Q.; Huang, R.; Guo, L.-H. One-step and high-density protein immobilization on epoxysilane-modified silica nanoparticles. *Chin. Sci. Bull.* **2009**, *54*, 2620–2626. [[CrossRef](#)]
27. Zhao, J.; Milanova, M.; Warmoeskerken, M.M.C.G.; Dutschk, V. Surface modification of TiO₂ nanoparticles with silane coupling agents. *Colloid. Surf. A Physicochem. Eng. Asp.* **2012**, *413*, 273–279. [[CrossRef](#)]
28. Lee, H.S.; Park, J.M.; Hwang, K.H.; Lim, H.M. Surface Functionalization of Zirconia Nanocrystals with Silane Coupling Agent and its Dispersion Behavior in O-Phenylphenoxyethyl Acrylate. *Mat. Sci. Forum.* **2018**, *922*, 20–25. [[CrossRef](#)]
29. Lu, H.T. Synthesis and characterization of amino-functionalized silica nanoparticles. *Colloid. J.* **2013**, *75*, 311–318. [[CrossRef](#)]

30. Iijima, M.; Sato, N.; Lenggoro, I.W.; Kamiya, H. Surface modification of BaTiO₃ particles by silane coupling agents in different solvents and their effect on dielectric properties of BaTiO₃/epoxy composites. *Colloid. Surf. A Physicochem. Eng. Asp.* **2009**, *352*, 88–93. [[CrossRef](#)]
31. Ha, T.T.; Canh, T.D.; Tuyen, N.V. A Quick Process for Synthesis of ZnO Nanoparticles with the Aid of Microwave Irradiation. *ISRN Nanotech.* **2013**, *2013*, 497873. [[CrossRef](#)]
32. Athauda, T.J.; Williams, W.; Roberts, K.P.; Ozer, R.R. On the surface roughness and hydrophobicity of dual-size double-layer silica nanoparticles. *J. Mater. Sci.* **2013**, *48*, 6115–6120. [[CrossRef](#)]
33. Turco, A. *Coloritura Verniciatura e Laccatura Del Legno*, 3rd ed.; Hoepli: Milan, Italy, 2005.
34. Weththimuni, M.L.; Canevari, C.; Legnani, A.; Licchelli, M.; Malagodi, M.; Ricca, M.; Zeffiro, A. Experimental characterization of oil-colophony varnishes: A preliminary study. *J. Int. Conserv. Sci.* **2016**, *7*, 813–826.
35. UNI EN 15886: 2010, *Conservazione dei Beni Culturali-Metodi di Prova-Misura del Aolore Delle Superfici*; UNI Ente Italiano di Unificazione: Milan, Italy, 2010.
36. UNI EN 15802:2010, *Conservazione dei Beni culturali-Metodi di Prova-Determinazione dell'Angolo di Contatto Statico*; UNI Ente Italiano di Unificazione: Milan, Italy, 2010.
37. Weththimuni, M.L.; Capsoni, D.; Malagodi, M.; Licchelli, M. Improving Wood Resistance to Decay by Nanostructured ZnO-Based Treatments. *J. Nanomater.* **2019**, *2019*, 6715756. [[CrossRef](#)]
38. Scalara, D.; Lazzari, M.; Chiantore, O. Ageing behaviour and pyrolytic characterization of diterpenic resins used as art materials: Colophony and venice turpentine. *J. Anal. Appl. Pyrolysis* **2002**, *64*, 345–361. [[CrossRef](#)]
39. Yu, Y.; Jiang, Z.; Wang, G.; Tian, G.; Wang, H.; Song, Y. Surface functionalization of bamboo with nanostructured ZnO. *Wood Sci. Technol.* **2012**, *46*, 781–790. [[CrossRef](#)]
40. ISO 15184:2012, *Paints and Varnishes—Determination of Film Hardness by Pencil Test*, 2nd ed.; International Organization for Standardization: Genève, Switzerland, 2012.
41. Grasset, F.; Saito, N.; Li, D.; Park, D.; Sakaguchi, I.; Ohashi, N.; Haneda, H.; Roisnel, T.; Mornet, S.; Duguet, E. Surface modification of zinc oxide nanoparticles by aminopropyltriethoxysilane. *J. Alloys Compd.* **2003**, *360*, 298–311. [[CrossRef](#)]
42. Sowa, H.; Ahsbahs, H. High-pressure X-ray investigation of zincite ZnO single crystals using diamond anvils with an improved shape. *J. Appl. Cryst.* **2006**, *39*, 169–175. [[CrossRef](#)]
43. Mueen, R.; Lerch, M.; Cheng, Z.; Konstantinov, K. Na-doped ZnO UV filters with reduced photocatalytic activity for sunscreen applications. *J. Mater. Sci.* **2020**, *55*, 2772–2786. [[CrossRef](#)]
44. Dippel, A.C.; Jensen, K.M.Ø.; Tyrsted, C.; Bremholm, M.; Bøjesen, E.D.; Saha, D.; Birgisson, S.; Christensen, M.; Billinge, S.J.L.; Iversen, B.B. Towards atomistic understanding of polymorphism in the solvothermal synthesis of ZrO₂ nanoparticles. *Acta Cryst.* **2016**, *A72*, 645–650.
45. Hernawan; Septawendar, R.; Sofiyarningsih, N.; Sutardi, S. The zirconia phase transformation in the preparation of nano zirconia by calcining a gel-emulsion precursor. *J. Ceram. Process. Res.* **2011**, *12*, 561–566.
46. Anandan, K.; Rajendran, V. A Low-temperature synthesis and characterization of tetragonal-ZrO₂ nanoparticles via simple hydrothermal process. *J. Phys. Sci.* **2013**, *17*, 179–184.
47. Manjunatha, S.; Dharmaprasanth, M.S. Synthesis and characterization of cerium doped ZrO₂ blue-green emitting nanophosphors. *Mater. Lett.* **2016**, *164*, 476–479. [[CrossRef](#)]
48. Guo, Z.; Wei, S.; Shedd, B.; Scaffaro, R.; Ereira, T.; Hahn, H. Particles surface engineering effect on the mechanical, optical and photoluminescent properties of ZnO/vinyl-ester resin nanocomposites. *J. Mater. Chem.* **2007**, *17*, 806–813. [[CrossRef](#)]
49. Nagaraju, G.; Udayabhanu, G.; Shivraj, P.; Prashanth, S.A.; Shastri, M.; Yathish, K.V.; Anupama, C.; Rangappa, D. Electrochemical heavy metal detection, photocatalytic, photoluminescence, biodiesel production and antibacterial activities of Ag-ZnO nanomaterial. *Mater. Res. Bull.* **2017**, *94*, 54–63. [[CrossRef](#)]
50. Ma, J.; Duan, L.; Lu, J.; Lyu, B.; Gao, D.; Wu, X. Fabrication of modified hydrogenated castor oil/GPTMSZnO composites and effect on UV resistance of leather. *Sci. Rep.* **2017**, *7*, 3742.
51. Schramm, C. High temperature ATR-FTIR characterization of the interaction of polycarboxylic acids and organotrialkoxysilanes with cellulosic material. *Spectroch. Acta A Mol. Biomol. Spectrosc.* **2020**, *243*, 118815. [[CrossRef](#)] [[PubMed](#)]
52. Fedtke, M.; Domaratiu, F. Curing of epoxide resins by anhydrides of dicarboxylic acids: Model reactions. *Polym. Bull.* **1986**, *15*, 13–19. [[CrossRef](#)]
53. Tang, J. Specific and irreversible inactivation of pepsin by substrate-like epoxides. *J. Biol. Chem.* **1971**, *246*, 4510–4517. [[CrossRef](#)]
54. Ross W., C.J. The reactions of certain epoxides in aqueous solutions. *J. Chem. Soc.* **1950**, 2257–2272. [[CrossRef](#)]
55. Goswami, D.N.; Kumar, S. Study on the curing of shellac with epoxy resins by dielectric measurements. *Angew. Makromol. Chem.* **1984**, *126*, 145–152. [[CrossRef](#)]
56. Fahim Ansari, M.; Sarkhel, G.; Nath Goswami, D.; Baboo, B. Coating properties of shellac modified with synthesised epoxidised-novolac resin. *Pigm. Resin Technol.* **2014**, *43*, 314–322. [[CrossRef](#)]
57. Clemens, R.J.; Rector, F.D. Synthesis of acetoacetyl—functional resins. *J. Coat. Technol.* **1989**, *61*, 83–91.
58. Lausecker, R.; Badilita, V.; Gleißner, U.; Wallrabe, U. Introducing natural thermoplastic shellac to microfluidics: A green fabrication method for point-of-care devices. *Biomicrofluidics* **2016**, *10*, 044101. [[CrossRef](#)]
59. Fahim Ansari, M.; Sarkhel, G.; Nath Goswami, D.; Baboo, B. Changes in the properties of shellac on blending with rosin, effect on storage. *Pigm. Resin Technol.* **2013**, *42*, 256–263. [[CrossRef](#)]

60. Thompson, A.C.; Vaughan, D. *X-ray Data Booklet*, 2nd ed.; University of California: Berkeley, CA, USA, 2001.
61. Younan, H.; Binghai, L.; Zhiqiang, M.; Teong, J. Studies and applications of standardless EDX quantification method in failure analysis of wafer fabrication. In Proceedings of the 15th International Symposium on the Physical and Failure Analysis of Integrated Circuits, Singapore, 7–11 July 2008.
62. Cristea, M.V.; Riedl, B.; Blanchet, P. Effect of addition of nanosized UV absorbers on the physico-mechanical and thermal properties of an exterior waterborne stain for wood. *Prog. Org. Coat.* **2011**, *72*, 755–762. [[CrossRef](#)]
63. Coelho, C.; Nanabala, R.; Meénager, M.; Commereuc, S.; Verney, V. Molecular changes during natural biopolymer ageing- The case of shellac. *Polym. Degrad. Stab.* **2012**, *97*, 936–940. [[CrossRef](#)]
64. Auclair, N.; Riedl, B.; Blanchard, V.; Blanchet, P. Improvement of photoprotection of wood coatings by using inorganic nanoparticles as ultraviolet absorbers. *For. Prod. J.* **2011**, *61*, 20–27. [[CrossRef](#)]
65. Wang, X.; Yang, F.; Yang, W.; Yang, X. A study on the antibacterial activity of one-dimensional ZnO nanowire arrays: Effects of the orientation and plane surface. *Chem. Commun.* **2007**, *42*, 4419–4421. [[CrossRef](#)] [[PubMed](#)]
66. Sharma, D.; Rajput, J.; Kaith, B.S.; Kaur, M.; Sharma, S. Synthesis of ZnO nanoparticles and study of their antibacterial and antifungal properties. *Thin Solid Films* **2010**, *519*, 1224–1229. [[CrossRef](#)]
67. Patra, P.; Mitra, S.; Debnath, N.; Goswami, A. Biochemical, biophysical, and microarray-based antifungal evaluation of the buffer-mediated synthesized nano zinc oxide: An in vivo and in vitro toxicity study. *Langmuir* **2012**, *28*, 16966–16978. [[CrossRef](#)] [[PubMed](#)]
68. Mohammed, D.Y. Detection the antifungal effect of zirconium oxide nanoparticles on mold which isolated from momestic's. *Al-Mustansiriyah J. Sci.* **2018**, *29*, 15–22.
69. Gowri, S.; Gandhi, R.R.; Sundrarajan, M. Structural, optical, antibacterial and antifungal properties of zirconia nanoparticles by biobased protocol. *J. Mater. Sci. Technol.* **2014**, *30*, 782–790. [[CrossRef](#)]